Journal of Sol-Gel Science and Technology
https://doi.org/10.1007/s10971-025-06700-0

ORIGINAL PAPER

# Controlled annealing for enhanced structural stability and luminescence of sol-gel synthesized $Gd_{2.37}Y_{0.6}Al_5O_{12}$: $Ce_{0.03}$ nanopowders

Karima Hammoum[1] · Samir Hamrit[2,3] · Allaoua Boukerika[4] · Lydia Zaidi[1] · Youssef Larbah[4] · Djamel Eddine Kdib[4]

Received: 5 January 2025 / Accepted: 10 February 2025
© The Author(s), under exclusive licence to Springer Science+Business Media, LLC, part of Springer Nature 2025

## Abstract

In this study, we report the synthesis of cerium-doped gadolinium yttrium aluminum garnet powders with chemical formula $Gd_{2.37}Y_{0.6}Al_5O_{12}$:$Ce_{0.03}$ via the sol-gel method. The effect of annealing temperature on the stability of the garnet phase was thoroughly investigated. Various characterization techniques, including X-ray diffraction (XRD), Fourier transform infrared spectroscopy (FTIR), field emission scanning electron microscopy (FESEM), and photoluminescence spectroscopy (PL), were employed to assess these effects. XRD analysis demonstrated a marked improvement in the stability and crystallinity of the garnet phase with increasing annealing temperatures. FESEM images revealed the evolution of interconnected quasi-spherical particles, with a significant enlargement in average particle size correlating with higher annealing temperatures. PL spectra displayed a broad emission band attributable to $Ce^{3+}$ transitions within the garnet matrix. Notably, the emission intensity exhibited a substantial enhancement with elevated annealing temperatures, which can be attributed to the increased crystallinity and a higher proportion of the garnet phase. These findings underscore the critical role of annealing temperature in optimizing the structural and luminescent properties of $Gd_{2.37}Y_{0.6}Al_5O_{12}$:$Ce_{0.03}$ nanopowders.

## Graphical abstract

The effect of annealing temperature on the stability of the garnet $Gd_{2.37}Y_{0.6}Al_5O_{12}$:$Ce_{0.03}$ and luminescence, structural, morphological properties.

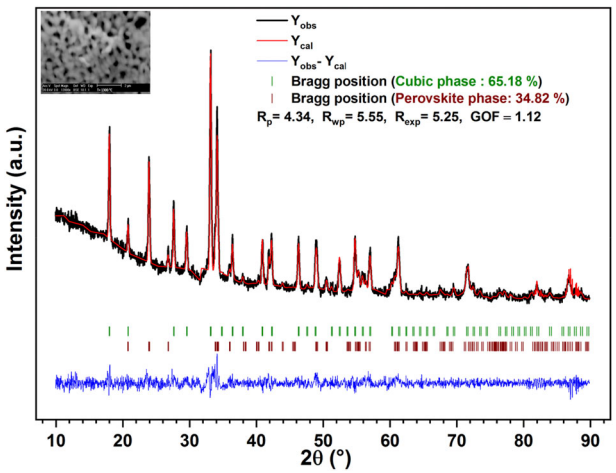


✉ Youssef Larbah
y.larbah@crna.dz

[1] Mechanics, Structures and Energetics Laboratory, University of Mouloud Mammeri Tizi-Ouzou (UMMTO), Tizi Ouzou, Algeria

[2] Physics Department, Faculty of Science, University of M'sila, 28000 M'sila, Algeria

[3] Laboratory of Materials Physics and Its Applications, University of M'sila, 28000 M'sila, Algeria

[4] Nuclear Research Center of Algiers (CRNA),02, Boulevard Frantz Fanon, B.P. 399, Algiers 16000, Algeria

Published online: 20 February 2025

**Keywords** GYAG: Ce · Sol-gel · Annealing effect · Stabilization · Photoluminescence

**Highlights**

- The effect of annealing temperature on the stability of the garnet $\mathbf{Gd_{2.37}Y_{0.6}Al_5O_{12}}$**: Ce**$_{0.03}$
- Luminescence properties of $\mathbf{Gd_{2.37}Y_{0.6}Al_5O_{12}}$**: Ce**$_{0.03}$ **Nanopowders**
- Stability of the garnet phase was obtained after heat treatment at 1300 °C
- Structural, morphological of $\mathbf{Gd_{2.37}Y_{0.6}Al_5O_{12}}$**: Ce**$_{0.03}$ **Nanopowders**

## 1 Introduction

In recent years, inorganic scintillators have become essential components in various ionizing radiation detection applications. Their ability to convert radiation energy into light makes them crucial components in several fields, including nuclear medicine, high-energy physics research, industrial radiation detection, environmental monitoring, homeland security, and space exploration [1–5]. Enhancing the scintillation and luminescence properties of these scintillating materials is essential for improving their effectiveness in detecting ionizing radiation. Among the various inorganic scintillators, cerium-doped gadolinium aluminum garnet ($Gd_3Al_5O_{12}$:$Ce^{3+}$), commonly referred to as GAG:Ce, has emerged as a promising material due to its exceptional scintillation properties. However, achieving a stable cubic garnet phase in GAG is challenging due to thermodynamic instability, which often leads to the coexistence of mixed phases, such as perovskite $GdAlO_3$ (GAP) and monoclinic $Gd_2Al_4O_9$ (GAM). Unlike the widely utilized yttrium aluminum garnet (YAG), gadolinium aluminum garnet (GAG) is less commonly employed as a host material due to the inherent challenges associated with its conventional synthesis methods. In recent years, there has been a surge in research interest surrounding cerium-doped gadolinium aluminum garnet ($Gd_3Al_5O_{12}$:$Ce^{3+}$). However, to the best of our knowledge, there is no reported $Ce^{3+}$-activated GAG compounds with a consistently stable cubic structure. Despite the growing interest in this compound, there remains a significant challenge in achieving a consistently stable cubic structure in $Ce^{3+}$-activated GAG compounds. Using GAG garnet as a matrix host offers the potential to create captivating transparent ceramics for scintillating materials [6]. Indeed, given the significantly higher atomic weight of Gd compared to Y, ensuring a high theoretical density in the material is essential for effective X-ray stopping power.

In the literature, it has been demonstrated that obtaining a pure garnet phase can be effectively achieved by partially substituting gadolinium with yttrium (Y) or lutetium (Lu) in the garnet host matrix, leading to enhanced luminescence properties [7, 8].

These compounds possess remarkable physical properties, including high luminous efficiency within the energy range of 48,000 to 56,000 photons/MeV, high density, rapid decay (approximately 52 ns), and high energy resolution [9–12]. Additionally, various synthesis methods have been employed to prepare garnet phosphors in a pure phase by ensuring uniform mixing of precursors. These methods include the sol-gel method [13], combustion method [14], co-precipitation method [15], hydrothermal method [16], and solvothermal method [17], Recent studies have comprehensively reviewed synthesis strategies for rare-earth-activated inorganic phosphors, highlighting the advantages and challenges of different techniques in achieving high phase purity and optimized luminescent properties [18]. Among these methods, the sol-gel process stands out for its straightforward operation, mild synthesis conditions, and ability to facilitate the production of mixed garnets in various forms while preserving outstanding homogeneity. In our prior research [19], we aimed to enhance the stability of the $Gd_3A_{l5}O_{12}$:$Ce^{3+}$ lattice host in its garnet phase using the sol-gel method. Our primary objective was to optimize two key synthesis parameters: the solution pH and the annealing temperature. The investigation of the structural properties of this lattice host revealed a significant 79% stabilization of the cubic structure, achieved at an annealing temperature of 1500 °C and a pH of 7 [19]. Furthermore, our results align with previous findings by Young Park et al. [20], who demonstrated successful stabilization of the garnet phase through the incorporation of 10 mol% Y ions and sintering temperatures ranging from 1000 to 1500 °C in GAG:Ce phosphors (GdYAG:Ce), synthesized using the solvothermal method. This study investigates the synthesis of the $(Gd_{1-x-z}Y_xCe_z)_3Al_5O_{12}$ structure, co-doped with a small amount of yttrium ($Y^{3+}$) at $x = 0.2$ and cerium ($Ce^{3+}$) at $z = 0.01$, corresponding to the composition $Gd_{2.37}Y_{0.6}A-l_5O_{12}$:$Ce_{0.03}$ (called GYAG:Ce) to enhance its structural stability and luminescent properties. Our objective is to investigate the influence of annealing temperature on the phase stability and luminescence efficiency of this composition. Huh et al. [21] reported that the this composition forms a pure garnet phase at 1550 °C. To our knowledge, limited research has been conducted on the effects of annealing temperature on this specific material when

synthesized via the sol-gel method. Therefore, this study provides valuable insights into the structural evolution, phase purity, and luminescence behavior of $Gd_{2.37}Y_{0.6}Al_5O_{12}:Ce_{0.03}$ phosphors as a function of thermal treatment.

## 2 Experimental

### 2.1 Samples preparation

$Gd_{2.37}Y_{0.6}Al_5O_{12}:Ce_{0.03}$ powders were prepared via the sol-gel protocol. The starting materials used in this study were obtained without further purification: $Gd_2O_3$ (99.99%) and $Ce(NO_3)_3{\cdot}6H_2O$ (99.99%) were purchased from Sigma-Aldrich (USA), $Al(NO_3)_3{\cdot}9H_2O$ (99.0%) was obtained from Biochem Chemopharma (Montreal, Quebec), nitric acid ($HNO_3$) was acquired from Merck (Germany), ethylene glycol (EG 1000), and acetic acid ($CH_3COOH$) were obtained from Biochem Chemopharma (France), and ammonia ($NH_4OH$) was acquired from Cheminova Internacional SA (Spain).

Initially, an amount of $Gd_2O_3$ oxide was dissolved in 1 mL of $HNO_3$ which was subsequently diluted with deionized water to obtain a total volume of 50 mL and agitated at 100 °C for 1 hour, resulting in the formation of a transparent solution. Appropriate amounts of yttrium nitrate ($Y(NO_3)_3{\cdot}6H_2O$), aluminum nitrate ($Al(NO_3)_3{\cdot}9H_2O$), and cerium nitrate ($Ce(NO_3)_3{\cdot}6H_2O$) were added to the solution, which was then stirred for 1 h until a transparent solution was obtained. Acetic acid ($CH_3COOH$) and ethylene glycol were introduced into the solution at a molar ratio of $AA:M^{3+}$ and $EG:M^{3+}$ of 1:1, where $M^{3+}$ represents the sum of $Gd^{3+}$, $Y^{3+}$, $Al^{3+}$, and $Ce^{3+}$ ions. These solutions have been stirred for 2 h and pH was adjusted to be 1 using ammonium hydroxide ($NH_4OH$). The resulting solutions were dried at 120 °C until xerogels were formed. Finally, the xerogels were annealed at 800, 900, 1100, 1300 and 1500 °C for 4 h in a programmable tube furnace. Figure 1

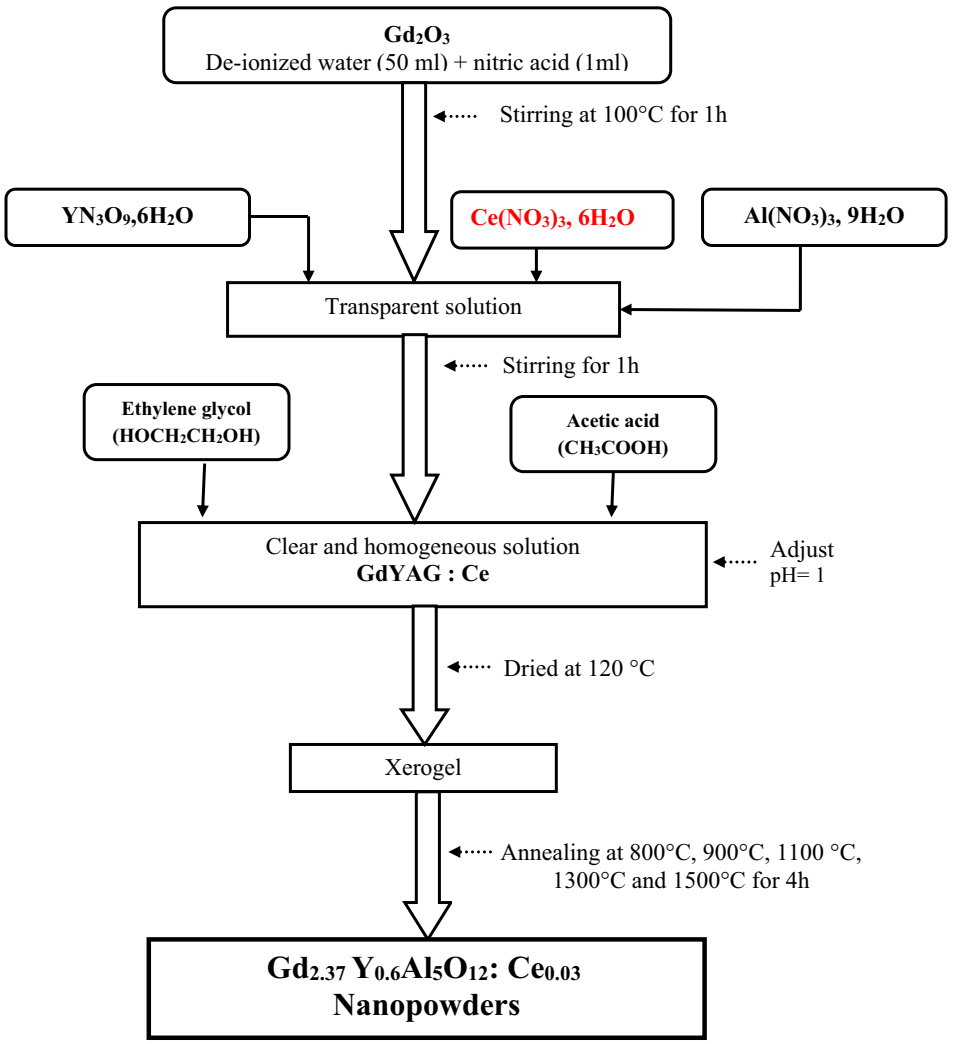


**Fig. 1** Synthesis protocol of GYAG:Ce nanopowders using a simple sol–gel method

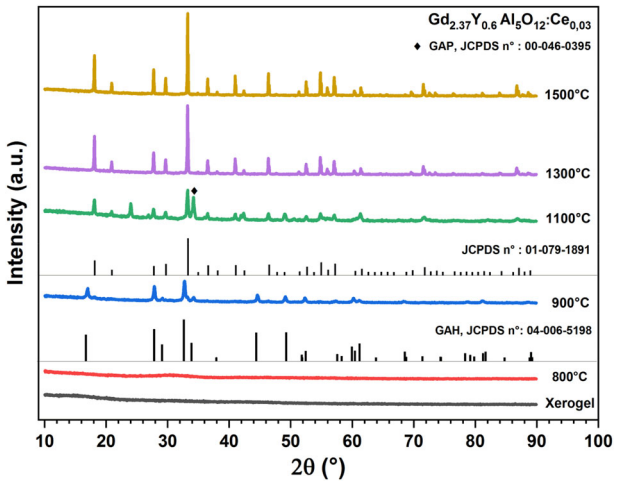


**Fig. 2** XRD patterns of GYAG:Ce nanpowders annealed at different temperatures

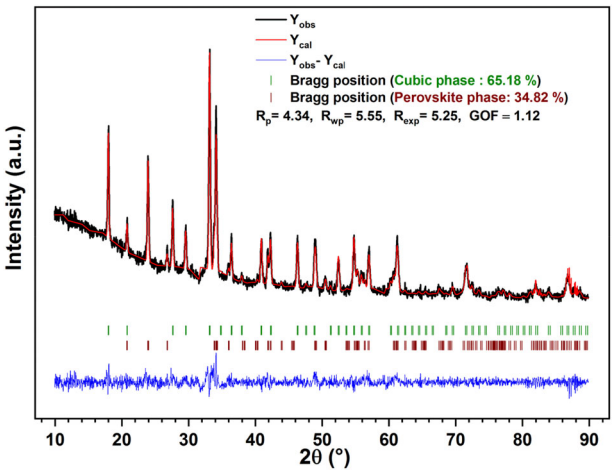


**Fig. 3** Rietveld refinement of GYAG:Ce nanopowder prepared at 1100 °C

displays the sol-gel protocol used in the synthesis of $Gd_{2.37}Y_{0.6}Al_5O_{12}$:$Ce_{0.03}$ powders.

### 2.2 Samples characterization

The structural analysis was conducted using X-ray diffraction (XRD) with a PANalytical X'Pert Pro (Philips) diffractometer, operating at 40 kV and 30 mA with Cu $K_\alpha$ radiation ($\lambda = 1.5425$ Å). The data of the synthesized samples were processed by Rietveld refinement using FullProf_Suite program [22, 23]. The infrared spectra were recorded in the range of 400–4000 $cm^{-1}$ with a Thermo Nicolet 380 Fourier transform infrared (FTIR) spectrometer. The morphology and chemical composition of samples were analyzed using a Philips XL 30 Field Emission Scanning Electron Microscope (FE-SEM) and Energy Dispersive X-ray (EDS) spectroscopy, respectively. Room temperature excitation and emission spectra were measured using a fluorescence spectrophotometer PerkinElmer LS-50B equipped with a pulsed Xenon lamp.

## 3 Results and discussions

### 3.1 Phase identification (https://ieeexplore.ieee.org/abstract/document/6102329/)

X-ray diffraction analysis was performed to explore the annealing effects on the evolution of the garnet phase, its proportion, and its structural characteristics. Figure 2 illustrates the XRD patterns of $Gd_{2.37}Y_{0.6}Al_5O_{12}$: $Ce_{0.03}$ nanopowders annealed at different temperatures (800, 900, 1100, 1300 and 1500 °C) for 4 h. For the as-prepared sample, the absence of any diffraction peaks in the XRD pattern confirms the amorphous nature of the obtained xerogel. After annealing at 800 °C, a broad band centered around $2\theta = 30°$ was observed, indicating that the nanopowder remains in an amorphous state. Following thermal treatment at 900 °C, well-defined diffraction peaks corresponding to the $GdAlO_3$ (GAH) hexagonal phase appeared, in accordance with JCPDS n°: 04-006-5198 standards, confirming the sample's crystallization at this temperature. Notably, no diffraction peaks characteristic of the garnet phase were detected. After annealing at 1100 °C, the hexagonal phase decomposed and transformed into two distinct phases: garnet (JCPDS 01-79-1891) and perovskite (JCPDS n° 00-046-0395), with proportions of 65.18% and 34.82%, respectively, calculated using Rietveld method (see the example presented in Fig. 3). Starting at 1300 °C, all diffraction peaks corresponded exclusively to the pure garnet phase (JCPDS 01-79-1891), with no secondary phases detected. These findings are in good agreement with the results reported by Chiang et al. [24] regarding $Gd_3Al_5O_{12}$ doped with various trivalent ions ($Tb^{3+}$, $Y^{3+}$, $Lu^{3+}$ and $Ga^{3+}$), synthesized via a precipitation method at different annealing temperatures. Additionally, raising the annealing temperature to 1500 °C resulted in the garnet phase achieving perfect stability, with narrower and well-separated diffraction peaks of increased intensity. This observation suggests an enhancement in the crystallinity of the sample at this annealing temperature [25].

The crystallite size of the synthesized $Gd_{2.37}Y_{0.6}Al_5O_{12}$:$Ce_{0.03}$ nanopowders was estimated using various methods, including the Scherrer method, Williamson-Hall (W-H) analysis, and Halder-Wagner (H-W) approaches. Additionally, Rietveld refinement was employed for further validation.

The Scherrer equation [26, 27] was used to estimate the crystallite size:

$$D_{sch} = \frac{0.9\lambda}{\beta COS\theta} \quad (1)$$

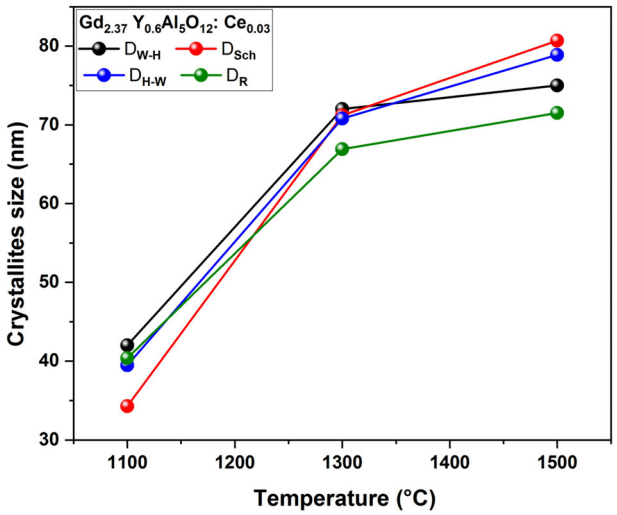


**Fig. 4** Evolution of crystallite size of GYAG:Ce nanopowders as a function of annealing temperature

where $\lambda$ is the wavelength of incident X-ray, $\beta$ is the FWHM measured in radians and $\theta$ is the Bragg angle of diffraction peak.

The Williamson-Hall method considers both size and strain effects on peak broadening and is expressed as [28] :

$$\frac{\beta COS\theta}{\lambda} = \frac{1}{D_{W-H}} + \varepsilon \frac{\sin\theta}{\lambda} \quad (2)$$

The Halder-Wagner approach refines the estimation of crystallite size and strain using the following equation [28, 29]:

$$\left(\frac{\beta^*}{d^*}\right)^2 = \frac{0.9}{D_{H-W}} \frac{\beta^*}{(d^*)^2} + (2\varepsilon)^2 \quad (3)$$

Where: $\beta^* = \frac{\beta \cos\theta}{\lambda}$ and $d^* = \frac{2 \sin\theta}{\lambda}$.

The crystallite size $(\mathbf{D_{H-W}})$ and microstrain $\boldsymbol{\varepsilon}$ are determined from the slope and intercept of the linear regression of $((x = \frac{\beta^*}{(d^*)^2}, y = (\frac{\beta^*}{d^*})^2))$.

From Fig. 4, it is evident that the crystallite size of the samples increases with rising annealing temperatures. Both the Williamson-Hall and Halder-Wagner methods provide crystallite size estimates nearly identical to those obtained by the Scherrer method, confirming that the broadening of the spectral lines is indeed due to size effects. Compared to peak-to-peak analyses methods ($D_{Sch}$, $D_{W-H}$, and $D_{H-W}$), the crystallite sizes obtained through the Rietveld method consistently show good agreement, with the order of magnitude being approximately the same. This reaffirms the utility of all four methods for estimating crystallite size in this study. According to the results presented in Table 1, the micro-strain values decrease with increasing annealing temperature. The negative strain values suggest the presence of lattice distortion or deformation [30, 31]. This trend aligns with the findings of Jiang et al. [32], who attributed similar behavior to lattice contraction. This correlation is consistent with the observed decrease in lattice parameter and volume as the annealing temperature increases. At high annealing temperatures, the decrease in micro-strain is associated with minimal distortion in the crystal lattice. The reduction in lattice parameter and the increase in crystallite size indicate a decrease in lattice interplanar spacing, potentially leading to an enhancement in lattice density and a lower density of defects. A similar behavior was noted by Boukerika et al. [33] in their investigation of the impact of annealing temperature on europium-doped $Y_2O_3$ prepared using the sol-gel method.

**Table 1** Summarizes the strain values determined by different methods, as well as the lattice parameter and its volume calculated by Rietveld method for the nanopowders annealed at different temperatures

| Samples $Gd_{2.37}Y_{0.6}Al_5O_{12}$: $Ce_{0.03}$ | $\varepsilon_{W-H}$ (%) | $\varepsilon_{H-W}$ (%) | $\varepsilon_R$ (%) | a (Å) | V (Å$^3$) |
|---|---|---|---|---|---|
| **T = 900 °C** | --- | --- | --- | --- | --- |
| **T = 1100 °C** | 0.0009 | 0.0008 | 0.2277 | 12.0972 | 1770.3529 |
| **T = 1300 °C** | −0.0013 | −0.0005 | 0.0908 | 12.0936 | 1768.7380 |
| **T = 1500 °C** | −0.0023 | −0.0006 | 0.0373 | 12.0902 | 1767.2635 |

## 3.2 Infrared spectroscopy analysis

To explore the changes in organic species as a function of thermal treatment in the garnet lattice, FTIR spectra were performed in the range of 400 to 4000 cm$^{-1}$. Figure 5a, b illustrate the FTIR spectra of both as-prepared and calcined nanopowders at varying temperatures, ranging from 800 to 1500 °C for 4 hours. In Fig. 5a, the spectrum reveals distinct bands corresponding to organic residues identified in the as-prepared sample. These bands can be categorized into three parts based on their energy range: the broad absorption band observed between 3000 and 3700 cm$^{-1}$, centered at 3400 cm$^{-1}$, originates from the vibrations of O-H bonds [34]. The bands identified around 1651 cm$^{-1}$ and 1300 cm$^{-1}$ are associated with the vibrations of C = O and C-O bonds, respectively, while the one at 823 cm$^{-1}$ is characteristic of C-C vibrations. The bands within the range of 400 to 800 cm$^{-1}$ are attributed to M-O vibrations and are not observed in the as-prepared sample, confirming the amorphous nature discussed in the XRD results.

Figure 5b presents the changes in organic compounds as a function of annealing temperatures. When comparing the sample annealed at 800 °C with the xerogel, identical absorption bands are observed, albeit with lower intensity. This observation confirms that the structure remains amorphous at this temperature. However, at 900 °C, the intensity

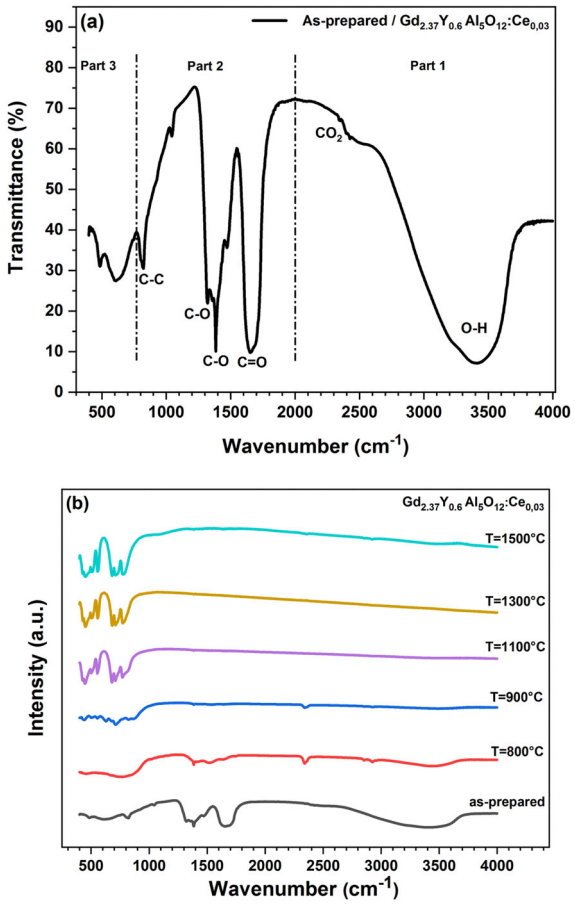


**Fig. 5** FTIR Spectrum of **a** as-prepared GYAG:Ce, **b** Comparison of FTIR spectra of nanopowders annealed at different temperatures

of bands associated with organic compounds decreases with rising annealing temperature, except for the persistent peak linked to $CO_2$, which remains due to the presence of air during the analysis. Additionally, bands with low intensity appear around 2850 $cm^{-1}$ and 2923 $cm^{-1}$, attributed to C-H bonds. Moreover, bands in the range of 400 to 800 $cm^{-1}$, characterizing M-O bonds, begin to appear from an annealing temperature of 900 °C or higher. This finding aligns well with the XRD analysis and confirms the crystallization of the sample from this annealing temperature.

### 3.3 Morphological characterization and elemental analysis

Figure 6 illustrates the evolution of particle morphology in the prepared samples as a function of calcination temperature. The results suggest a significant impact of thermal treatment on particle morphology. Specifically, the sample annealed at 900 °C exhibits a porous structure with an estimated mean pore size of 465 nm (see Fig. 6a). As the annealing temperature increases to 1100 °C, the pore size decreases, and the synthesized powder demonstrates a morphology characterized by very small particles and a reduced degree of agglomeration (refer to Fig. 6b). At annealing temperatures of 1300 °C and 1500 °C, the particles undergo considerable growth, forming interconnected quasi-spheres with an increasing degree of agglomeration (see Fig. 6c, d). As these particles are well defined, their distribution was determined from SEM micrographs using

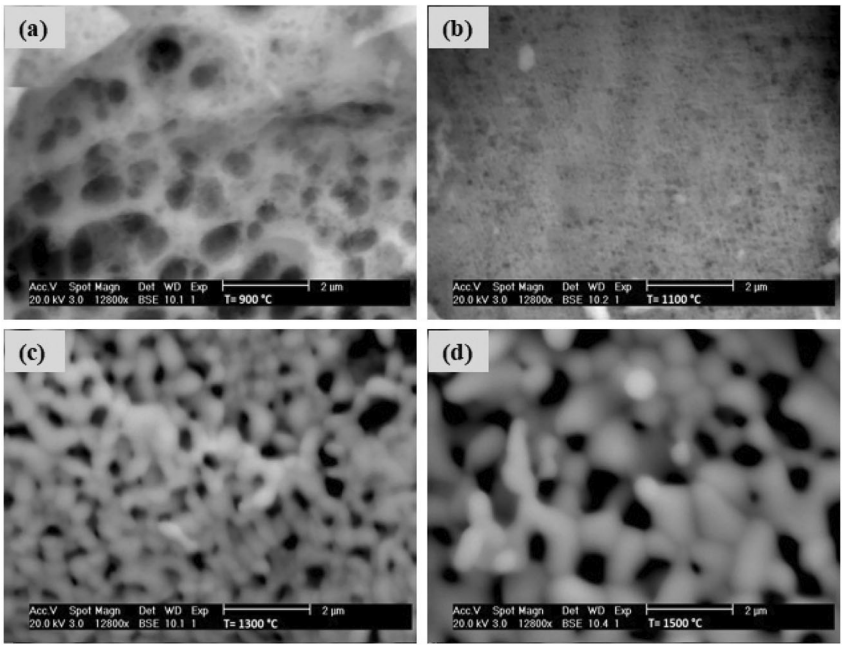


**Fig. 6** SEM image of GYAG:Ce nanopowder annealed at different temperatures

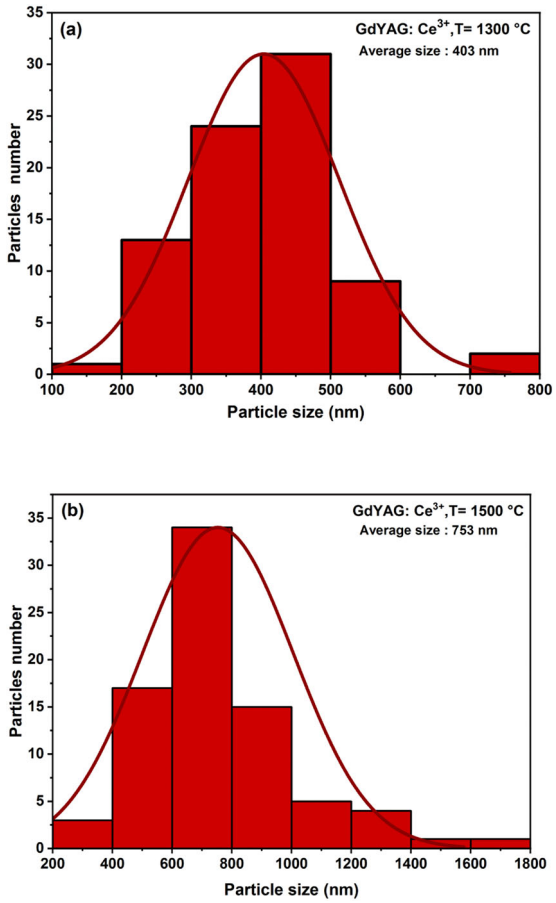


**Fig. 7** Distributions of particle size for samples annealed at **a** 1300 °C and **b** 1500 °C

ImageJ software, and the results are presented in Fig. 7. It is evident that the particles exhibit a broad size distribution. Additionally, the mean particle size significantly increases with rising annealing temperatures, from 403 nm at 1300 °C to 753 nm at 1500 °C. During thermal annealing, intensified agglomeration between particles leads to an increase in particle size and the formation of adhesion between them [35].

The EDS spectra of the samples annealed at 1300 °C and 1500 °C, along with their atomic composition, are depicted in Fig. 8a, b. Notably, the powder annealed at 1300 °C shows the same elements as the one annealed at 1500 °C, specifically Gd, Y, Al, and O. Additionally, the atomic ratios Gd:Al, Y:Al, and Y:Gd, assessed at 0.5, 0.1, and 0.2, respectively, align with the theoretical values.

### 3.4 Photoluminescence spectroscopy study

Figure 9 illustrate the excitation and emission spectra of $Gd_{2.37}Y_{0.6}Al_5O_{12}$: $Ce_{0.03}$ samples, synthesized using the sol-gel method and calcined at different annealing temperature ranging from 800 to 1500 °C. In each excitation spectrum (Fig. 9a), there are two absorption bands: a broad band ranging from 200 to 260 nm, attributed to lattice host absorption, and a second, low-intensity band around 279 nm, associated with the $^8S_{7/2} \rightarrow {}^6I_{7/2}$ transition of $Gd^{3+}$ ions. Additionally, the excitation spectra reveal a prominent band at approximately 465 nm and a secondary, lower-intensity band at around 341 nm. These bands are ascribed

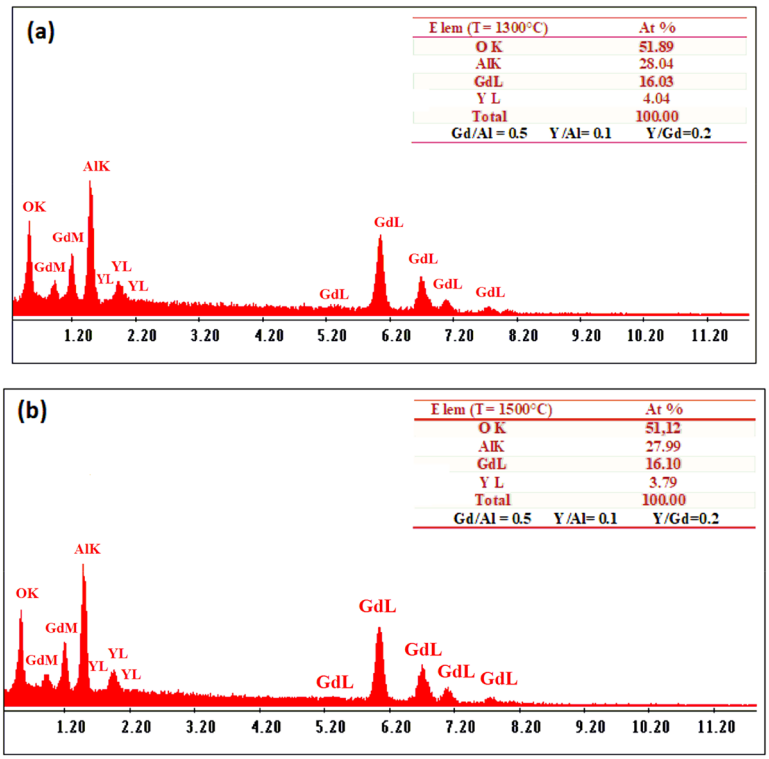


**Fig. 8** EDS analysis of samples annealed at **a** 1300 °C and **b** 1500 °C

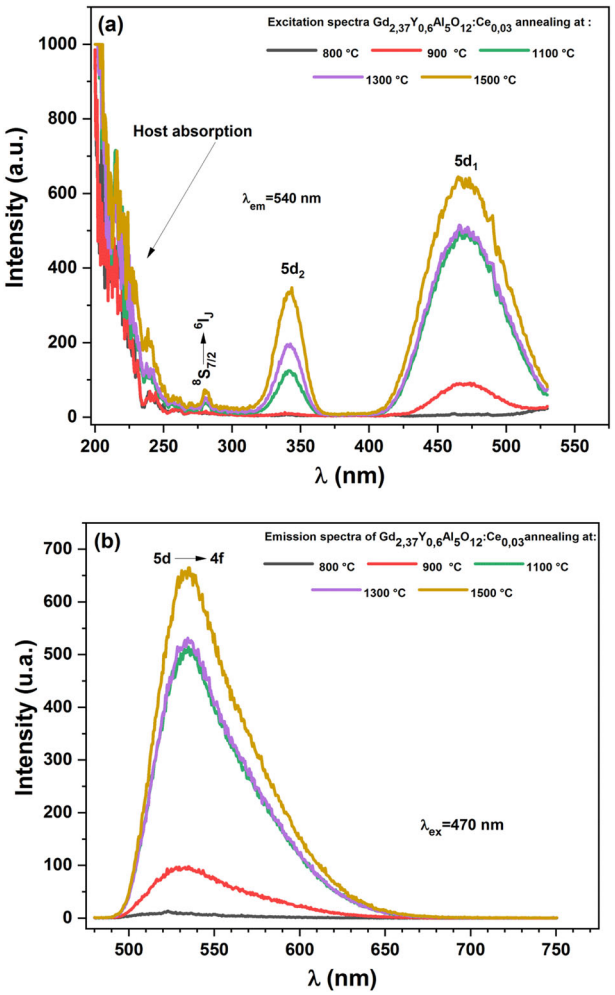


**Fig. 9** Photoluminescence spectra of GYAG:Ce nanopowders : **a** excitation spectra, **b** emission spectra

to the $4f \rightarrow 5d_1$ and $4f \rightarrow 5d_2$ transitions of $Ce^{3+}$ ions, respectively. These last two bands were not observed in the sample annealed at 800 °C, indicating that the GYAG matrix remained in an amorphous state at this temperature.

As the temperature increases to 900 °C, the characteristic absorption bands of $Ce^{3+}$ become apparent, albeit with low intensity. This is attributed to the mixed phase of this sample and the significant presence of the OH group, which partially extinguishes luminescence (light trapping centers), leading to lower emission [36]. The emission spectra (Fig. 9b) reveal a significant band around 530 nm, characteristic of the $Ce^{3+}$ ions, which intensifies as the temperature increases beyond 900 °C. This increase in emission intensity is attributed to improved crystallinity and the reduction of surface defects [37]. The gradual enhancement of luminescence with increasing temperature underscores the critical role of optimal annealing in achieving desirable luminescent properties, confirming that higher temperatures facilitate the formation of a well-crystallized phase with fewer luminescence-quenching defects. These findings emphasize the importance of precise temperature control during calcination to achieve optimal luminescent performance in $Gd_{2.37}Y_{0.6}Al_5O_{12}:Ce_{0.03}$. Similar trends have been observed in various studies [37–39]. As the annealing temperature increases, a systematic enhancement in emission intensity is observed. This increase is primarily attributed to two key factors: Increased Crystallinity; higher annealing temperatures promote grain growth and reduce structural defects, leading to fewer non-radiative recombination centers. The improved crystallinity enhances energy transfer efficiency within the lattice, thereby increasing luminescence intensity. Higher Proportion of the Garnet Phase; as demonstrated in the XRD analysis, the phase evolution follows a progressive transformation, with mixed phases ($GdAlO_3$ and $Gd_2Al_4O_9$) present at 900 °C and 1100 °C, while a pure garnet phase is achieved at 1300 °C and beyond. The luminescence of $Ce^{3+}$ ions are strongly dependent on their incorporation into the garnet lattice, as non-garnet phases introduce structural distortions that hinder radiative recombination. The higher proportion of the garnet phase at elevated temperatures provides an ideal host matrix for $Ce^{3+}$ ions, resulting in enhanced emission efficiency. Furthermore, at 1300 °C and 1500 °C, where the garnet phase is fully stabilized, the luminescence intensity reaches its maximum, indicating that both crystallinity and phase purity are crucial for optimizing the optical properties of the material.

These results confirm that the observed luminescence enhancement is not solely due to increased crystallinity but is also strongly correlated with the phase transformation into a pure garnet structure, which provides a highly efficient environment for $Ce^{3+}$ luminescence.

## 4 Conclusions

The nanopowders $Gd_{2.37}Y_{0.6}Al_5O_{12}$: $Ce_{0.03}$ were synthesized via the sol-gel method, and the influence of annealing temperature on the stability of the garnet phase was investigated. Through X-ray diffraction analysis and photoluminescence studies, it was observed that the degree of crystallinity improves with increasing annealing temperature. Specifically, the garnet phase was obtained after heat treatment at 1300 °C, accompanied by a gradual increase in emission intensity with annealing temperature. This enhancement in crystallinity correlates with the repair of non-radiative recombination sites at higher temperatures, leading to strong luminescence. These results collectively highlight the beneficial effects of higher annealing temperatures in enhancing the structural and luminescent properties of the synthesized nanopowders.

**Author contributions** Authorship contribution statement Author names: Karima Hammouma, Samir Hamritb,c, Allaoua Boukerikad,*, Lydia. Zaidia, Youssef Larbahd, and D.E. Kdib. Karima Hammoum: Investigation, Writing – original draft, Writing – review & editing.Samir Hamrit: Data curation, Software. A. Boukerika: Conceptualization, Data curation, Investigation, Validation, Resources, Writing – original draft, Writing – review & editing. L. Zaidi: Data curation, Methodology, Formal analysis, Investigation, Writing – original draft.Y. Larbah: Data curation, Methodology, Software, Writing – review & editing. D.E. Kdib : Data curation, Software.

## Compliance with ethical standards

**Conflict of interest** The authors declare that they have no conflict of interest.

## References


1. Gerasymov I, Nepokupnaya T, Boyarintsev A et al. (2020) GAGG:Ce composite scintillator for X-ray imaging. Opt Mater 109:110305. https://doi.org/10.1016/j.optmat.2020.110305
2. Lim JH, Park K, Kim HD et al. (2019) Potential of GAGG:Ce scintillation crystals for synchrotron X-Ray micro-imaging. Curr Appl Phys 19:303–307. https://doi.org/10.1016/j.cap.2018.12.011
3. Moses WW (2003) Time of flight in PET revisited. IEEE Trans Nucl Sci 50:1325–1330. https://doi.org/10.1109/TNS.2003.817319
4. Fong C, Dong AW, Hill AJ et al. (2015) Positron annihilation lifetime spectroscopy (PALS): A probe for molecular organisation in self-assembled biomimetic systems. Phys Chem Chem Phys 17:17527–17540. https://doi.org/10.1039/c5cp01921d
5. Iwanowska J, Swiderski L, Szczesniak T et al. (2013) Performance of cerium-doped Gd3Al2Ga 3O12 (GAGG:Ce) scintillator in gamma-ray spectrometry. Nucl Instruments Methods Phys Res Sect A Accel Spectrom Detect Assoc Equip 712:34–40. https://doi.org/10.1016/j.nima.2013.01.064
6. Liu G, Wang B, Li J et al. (2021) Research progress of gadolinium aluminum garnet based optical materials. Phys B Condens Matter 603:412775. https://doi.org/10.1016/j.physb.2020.412775
7. Sun Z, Chen Z, Wang M, Lu B (2020) Production and optical properties of Ce3+-activated and Lu3+-stabilized transparent gadolinium aluminate garnet ceramics. J Am Ceram Soc 103:809–818. https://doi.org/10.1111/jace.16776
8. Kucera M, Hanus M, Onderisinova Z et al. (2014) Energy transfer and scintillation properties of Ce3+ doped $(LuYGd)_3(AlGa)_5O_{12}$ multicomponent garnets. IEEE Trans Nucl Sci 61:282–289. https://doi.org/10.1109/TNS.2013.2281234
9. Nikl M, Mihoková E, Mareš JA et al. (2000) Traps and timing characteristics of LuAG:Ce3+ scintillator. Phys Status Solidi Appl Res 181:10–12. 10.1002/1521-396X(200009)181:1<R10::AID-PSSA999910>3.0.CO;2-9
10. Nikl M, Yoshikawa A, Kamada K et al. (2013) Development of LuAG-based scintillator crystals - A review. Prog Cryst Growth Charact Mater 59:47–72. https://doi.org/10.1016/j.pcrysgrow.2013.02.001
11. Kamada K, Endo T, Tsutumi K et al. (2011) Composition engineering in cerium-doped $(Lu,Gd)_3(Ga,Al)_5O_{12}$ single-crystal scintillators. Cryst Growth Des 11:4484–4490. https://doi.org/10.1021/cg200694a
12. Kamada K, Kurosawa S, Prusa P et al. (2014) Cz grown 2-in. size $Ce:Gd_3(Al,Ga)_5O_{12}$ single crystal; Relationship between Al, Ga site occupancy and scintillation properties. Opt Mater 36:1942–1945. https://doi.org/10.1016/j.optmat.2014.04.001
13. Carvalho IDS, Amanda AI, Silva AJS et al. (2019) Structural and photoluminescence properties of Eu 3+ -doped (Y 2.99-x Gd x) $Al_5O_{12}$ phosphors under vacuum ultraviolet and ultraviolet excitation. Mater Chem Phys 228:9–14. https://doi.org/10.1016/j.matchemphys.2019.02.035
14. Zhao C, Yu J, Zhang Y et al. (2020) Microwave-induced solution combustion synthesis and luminescent properties of nano-sized powders with different Nd concentrations. Ceram Int 46:17891–17895. https://doi.org/10.1016/j.ceramint.2020.04.096
15. Sun S, Xu Q (2012) Effect of calcination temperature on phase transformation and microstructure of Al2O3/GdAlO3 compound powder prepared by Co-precipitation method. Key Eng Mater 512–515:535–538
16. Xu M, Zhang Z, Zhao J et al. (2015) Low temperature synthesis of monodispersed YAG:Eu crystallites by hydrothermal method. J Alloys Compd 647:1075–1080. https://doi.org/10.1016/j.jallcom.2015.06.220
17. Park JY, Jung HC, Raju GSR et al. (2013) Solvothermal synthesis and luminescence properties of the novel aluminum garnet phosphors for WLED applications. Curr Appl Phys 13:441–447. https://doi.org/10.1016/j.cap.2012.09.001
18. Sitender S, Divender S, Preeti S et al. (2024) Synthesis strategies for rare earth activated inorganic phosphors: a mini review. Appl Res 4:1–18. https://doi.org/10.1002/appl.202400190
19. Zaidi L, Boukerika A, Larbah Y et al. (2022) Phase stabilization and luminescence properties of $Gd_3Al_5O_{12}$: Ce nanopowders prepared by Pechini method: Effect of pH and annealing temperature. Mater Chem Phys 286:126182. https://doi.org/10.1016/j.matchemphys.2022.126182
20. Park JY, Jung HC, Seeta Rama Raju G et al. (2009) Sintering temperature effect on structural and luminescence properties of 10 mol% Y substituted $Gd_3Al_5O_{12}$:Ce phosphors. Opt Mater 32:293–296. https://doi.org/10.1016/j.optmat.2009.08.004
21. Huh YD, Cho YS, Do YR (2002) The optical properties of (Y1-xGdx)3-z (Al1-yGay)5O12:Cez phosphors for white LED. Bull Korean Chem Soc 23:1435–1438
22. Rodríguez-Carvajal J (2001) Recent developments of the program FULLPROF, in Commission on Powder Diffraction (IUCr). Newsletter 26:12–19
23. Roisnel T, Rodríguez-Carvajal J (2001) WinPLOTR: a Windows tool for powder diffraction patterns analysis. Mater Sci Forum 378–381:118–123
24. Chiang C-C, Tsai M-S, Hon M-H (2007) Preparation of cerium-activated GAG phosphor powders. J Electrochem Soc 154:J326. https://doi.org/10.1149/1.2768900
25. Gotoh T, Jeem M, Zhang L et al. (2020) Synthesis of yellow persistent phosphor garnet by mixed fuel solution combustion synthesis and its characteristic. J Phys Chem Solids 142:109436. https://doi.org/10.1016/j.jpcs.2020.109436
26. Singh S, Singh D (2021) Structural and optical properties of green-emitting $Y_2SiO_5$:Tb3+ and Gd2SiO5:Tb3+ nanoparticles for modern lighting applications. Rare Met 40:3289–3298. https://doi.org/10.1007/s12598-020-01585-0
27. Singh S, Singh D (2021) Down-conversion and structural characterizations of trivalent terbium-doped garnet nanocrystalline phosphors for lighting applications. J Mater Sci Mater Electron 32:17674–17685. https://doi.org/10.1007/s10854-021-06303-9
28. Nath D, Singh F, Das R (2020) X-ray diffraction analysis by Williamson-Hall, Halder-Wagner and size-strain plot methods of CdSe nanoparticles- a comparative study. Mater Chem Phys 239:122021. https://doi.org/10.1016/j.matchemphys.2019.122021
29. Patel K, Patel A, Jethwa VP et al. (2024) X-ray diffraction analysis of orthorhombic SnSe nanoparticles by Williamson–Hall, Halder–Wagner and Size–Strain plot methods. Chem Phys Impact 8:100547. https://doi.org/10.1016/j.chphi.2024.100547

30. Prabhu RR, Khadar MA (2008) Study of optical phonon modes of CdS nanoparticles using Raman spectroscopy. Bull Mater Sci 31:511–515. https://doi.org/10.1007/s12034-008-0080-7
31. Gu F, Wang SF, Lü MK, Zhou GJ, Yuan DR (2004) Photoluminescence properties of $SnO_2$ nanoparticles synthesized by sol −gel method. J Phys Chem B 108:8119–8123. https://doi.org/10.1021/jp036741e
32. Jiang Q, Liang LH, Zhao DS (2001) Lattice contraction and surface stress of fcc nanocrystals. J Phys Chem B 105:6275–6277. https://doi.org/10.1021/jp010995n
33. Boukerika A, Guerbous L (2014) Annealing effects on structural and luminescence properties of red Eu 3+-doped Y2O3 nanophosphors prepared by sol-gel method. J Lumin 145:148–153. https://doi.org/10.1016/j.jlumin.2013.07.037
34. Ma S, Liu B, Cao B et al. (2020) Study on synthesis and luminescent properties of Mn4+ doped (Gd,Y)3Al5O12 phosphor. Opt Mater 102:109815. https://doi.org/10.1016/j.optmat.2020.109815
35. Korzhik M, Alenkov V, Buzanov O et al. (2019) Nanoengineered $Gd_3Al_2Ga_3O_{12}$ Scintillation materials with disordered garnet structure for novel detectors of ionizing radiation. Cryst Res Technol 54:1–10. https://doi.org/10.1002/crat.201800172
36. Dai Z, Boiko V, Grzeszkiewicz K et al. (2021) Effect of annealing temperature on persistent luminescence of Y3Al2Ga3O12:Cr3+ co-doped with Ce3+ and Pr3+. Opt Mater 111:. https://doi.org/10.1016/j.optmat.2020.110522
37. Liu P, Liu Y, Cui C et al. (2018) Enhanced luminescence and afterglow by heat-treatment in reducing atmosphere to synthesize the Gd3Al2Ga3O12: Ce3+ persistent phosphor for AC-LEDs. J Alloys Compd 731:389–396. https://doi.org/10.1016/j.jallcom.2017.10.037
38. Singh S, Simantilleke AP, Singh D (2021) Crystal structure and photoluminescence investigations of Y3Al5O12:Dy3+ nanocrystalline phosphors for WLEDs. Chem Phys Lett 765:138300. https://doi.org/10.1016/j.cplett.2020.138300
39. Gupta I, Singh S, Bhagwan S, Singh D (2021) Rare earth (RE) doped phosphors and their emerging applications: A review. Ceram Int 47:19282–19303. https://doi.org/10.1016/j.ceramint.2021.03.308

**Publisher's note** Springer Nature remains neutral with regard to jurisdictional claims in published maps and institutional affiliations.

Springer Nature or its licensor (e.g. a society or other partner) holds exclusive rights to this article under a publishing agreement with the author(s) or other rightsholder(s); author self-archiving of the accepted manuscript version of this article is solely governed by the terms of such publishing agreement and applicable law.